


RESEARCH

Open Access



Combination tanning mechanism inspired environmentally benign catalyst for efficient degradation of tetracycline

Meng Xiao¹, Shuangmei Liu¹, Wenqian Qi¹, Yu Peng², Qingyu Yan³ and Hui Mao^{1*} 

Abstract

The utilization of chelation reaction between metals and tannins is a common tanning method in leather chemistry. Herein, a novel combination tanning mechanism inspired environmentally benign catalyst (CMBT-Fe⁰) was synthesized by immobilizing Fe nanoparticles onto bayberry tannin (BT) grafted chitosan microfibers (CM). The obtained catalyst featured a well-defined microfibrillar structure, on which Fe⁰ nanoparticles were highly dispersed to exhibit exceptional catalytic activity for the degradation of tetracycline (TC). The catalytic activity of CMBT-Fe⁰ was 1.72 times higher than that of the commercial Fe⁰ nanoparticles without immobilization, with 95.03% of TC degraded within 90.0 min. The CMBT-Fe⁰ catalysts were recycled 6 times, with the removal rate of TC maintained at 82.56%. Furthermore, a possible mechanism responsible for the catalytic removal of TC was provided by analyzing the catalytic degradation products via liquid chromatography-mass spectrometry. Therefore, our investigation successfully developed efficient catalysts to address the concerned environmental issue of antibiotic pollution.

Keywords Vegetable tannin, Combination tanning, Environmental catalyst, Tetracycline degradation

*Correspondence:

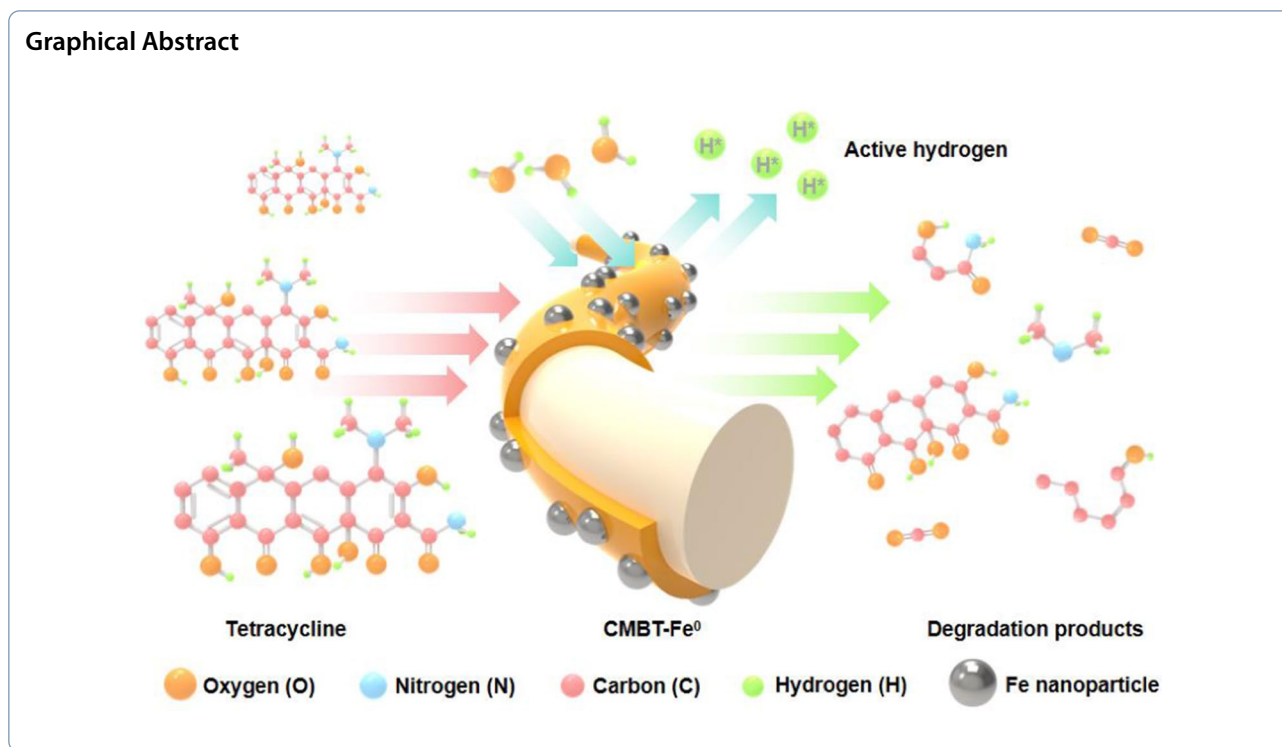
Hui Mao

rejoice222@163.com

Full list of author information is available at the end of the article



© The Author(s) 2023. **Open Access** This article is licensed under a Creative Commons Attribution 4.0 International License, which permits use, sharing, adaptation, distribution and reproduction in any medium or format, as long as you give appropriate credit to the original author(s) and the source, provide a link to the Creative Commons licence, and indicate if changes were made. The images or other third party material in this article are included in the article's Creative Commons licence, unless indicated otherwise in a credit line to the material. If material is not included in the article's Creative Commons licence and your intended use is not permitted by statutory regulation or exceeds the permitted use, you will need to obtain permission directly from the copyright holder. To view a copy of this licence, visit <http://creativecommons.org/licenses/by/4.0/>.



1 Introduction

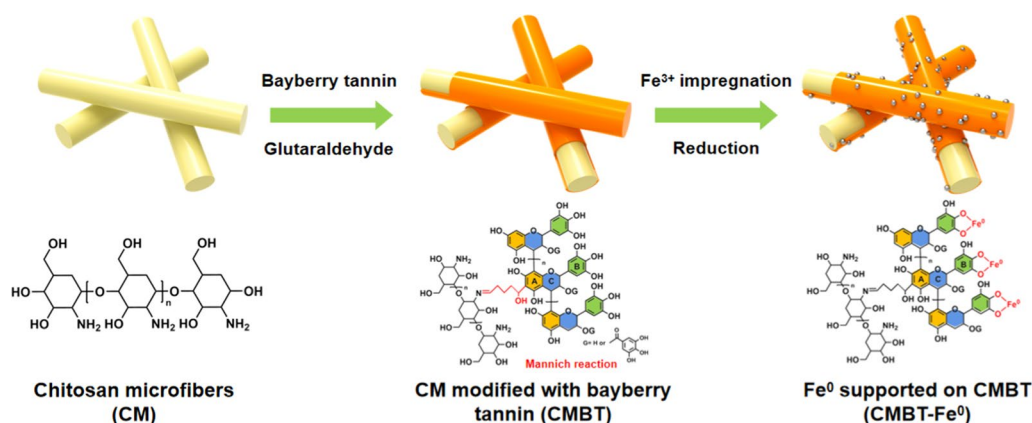
Tetracycline (TC) is one of the broad-spectrum antibiotics that have been widely used in human therapy and veterinary medicine [1]. TC discharged in wastewater could cause a series of negative influences to human health and ecological safety, including a variety of toxic effects, bacterial antibiotic resistance [2, 3]. Various technologies have been developed to deal with TC pollution in water, such as adsorption, electron pulse radiolysis, photocatalysis and biological methods [4–7]. Among them, nanoscale zero-valent iron (Fe⁰) technology has emerged as one of the most promising alternatives due to its high efficiency, affordability, and non-toxic nature [8, 9].

Fe⁰ catalysts are able to degrade various antibiotics via either a Fenton-like oxidation mechanism or a reduction mechanism [10, 11]. However, the agglomeration and Fe³⁺ leakage of Fe⁰ catalysts unfortunately result in a loss of reactivity and hinder their interactions with surrounding media [12, 13]. Various inorganic and organic supporting matrices have been investigated to stabilize Fe⁰ nanoparticles, such as diatomite [14], bentonite [15], PVP [16], polydopamine [17], carboxymethyl cellulose [18] and starch [19]. However, physical interactions with the inorganic supporting matrices are usually ineffective to prevent the aggregation or leaching of Fe⁰ nanoparticles, while the organic polymers cannot solve the problems such as over encapsulation-caused low activity of catalytic sites, which often leads to poor catalytic

performances [20–23]. To overcome these disadvantages, a novel multifunctional support matrix is required to stabilize Fe⁰ nanoparticles in an appropriate manner. In this regard, natural polymer materials with abundant functional groups and unique molecular configurations are promising alternatives.

Chitosan is a natural polymer material abundant in hydroxyl and amino groups, which is produced from the deacetylation of chitin, the second most abundant polysaccharide in nature after cellulose [24]. Chitosan has excellent biocompatibility and biodegradability, which is able to be processed into chitosan microfibers (CM) to gain efficient mass transport kinetics [25]. Therefore, CM is a promising matrix to immobilize Fe⁰ nanoparticles for developing heterogeneous Fe⁰ nanoparticle catalysts. However, CM is soluble in dilute acids, which requires the improvement of stability in solutions [26]. Moreover, it is preferred to enhance the affinity of CM to metal species for preventing any migration and agglomeration of Fe⁰ nanoparticles.

Vegetable tannins are a class of water-soluble polyphenols with the molecular weight in the range of 500–3000 Da, which are rich in various plant biomasses, such as leaves, roots and barks. Vegetable tannins are multifunctional natural polymers due to their abundant phenolic hydroxyl groups, which enable them to display high affinity towards metal ions via chelation [27]. Actually, vegetable tannins are utilized as tanning



Scheme 1 Schematic illustration showing the synthesis procedure of CMBT-Fe⁰

agents with the combination of metals in the leather industry. The as-developed combination tanning methods have been conventionally utilized in leather manufacture, which taken the advantage of the chelation ability of vegetable tannins with metal ions (e.g., Al³⁺) for significantly enhancing the bridged linkage degree of tanned leather. Great efforts have been dedicated to developing combination tanning techniques [28]. These previous investigations to combination tanning inspired us that the remarkable chelation-based affinity of vegetable tannins to metal ions species is possible to be applied in realizing the immobilization of metal species, such as Fe⁰ nanoparticles with the high dispersity onto the supporting matrix of CM.

Based on the above idea, bayberry tannin (BT), a typical condensed tannin, was utilized to modify chitosan microfibers (CM). The 6 and 8 positions of the A rings of BT exhibited high nucleophilic reaction activities, which allowed their covalent bonding to the amino groups of CM via reactions with aldehydes (e.g., glutaraldehyde) [29]. The resulting CMBT (chitosan microfibers modified with bayberry tannin) well preserved the well-defined fibrous structure, which further realized the impregnation of Fe³⁺ via the chelation with BT covalently bound on the surface of CM. Moreover, the covalent-bond interactions between BT and CM inhibited the dissolution of CM in acid solutions, providing with significantly enhanced material stability. After the reduction of Fe³⁺ on the CMBT, a novel environmentally benign catalyst, CMBT supported Fe⁰ nanoparticles (CMBT-Fe⁰) was successfully prepared (Scheme 1). We systematically investigated the performances of CMBT-Fe⁰ for the catalytic removal of TC, including the effect of initial pH, initial concentration of TC and temperature. Moreover, the catalytic degradation mechanism of TC by the CMBT-Fe⁰ was also discussed.

2 Experimental sections

2.1 Materials

Chitosan microfibers were received from Tianjin Glory Tang Technology Co., Ltd. (China). Bayberry tannin was obtained from the plant of forest product in Guangxi province (China). Iron (III) chloride hexahydrate (FeCl₃·6H₂O), sodium borohydride (NaBH₄), tetracycline (TC), commercial Fe⁰ nanoparticles and all of other chemicals were of analytical grade, which were purchased from Aladdin Co., Ltd. (China). Deionized water was used throughout the experiments.

2.2 Preparation of CMBT-Fe⁰

1.60 g of bayberry tannin was dissolved in 100.0 mL of deionized water. 4.0 g of chitosan fibers were immersed in the above tannin solution and stirred at 25 °C for 2 h. Subsequently, 5.0 mL of glutaraldehyde solution (v/v, 50%) was added into the above mixture at pH 6.0, which was then reacted for 6.0 h at 40 °C. After the solid–liquid separation and washing, the collected solids were dried at 60 °C for 24 h to obtained CMBT.

0.55 g CMBT was added into 30.0 mL of Fe³⁺ solution (FeCl₃·6H₂O, 16.70 mg/mL) at 25 °C and stirred for 90 min. Then 12.0 mL of NaBH₄ (10.00 mg/mL) solution was slowly dropwised into the above mixture. After stirring for 1.0 h, the CMBT-Fe⁰ was separated, followed by washing with distilled water and subsequent drying.

2.3 Catalytic degradation experiments

The catalyst dose was fixed at 55.0 mg for all degradation experiments. The influences of experimental conditions on the degradation of TC were investigated by changing several key parameters, including the initial pH of antibiotic solution (2.0–9.0), the initial concentration of TC (40.0–120.0 mg/L) and temperature (288–303 K). The sample was collected by a disposable syringe, which was

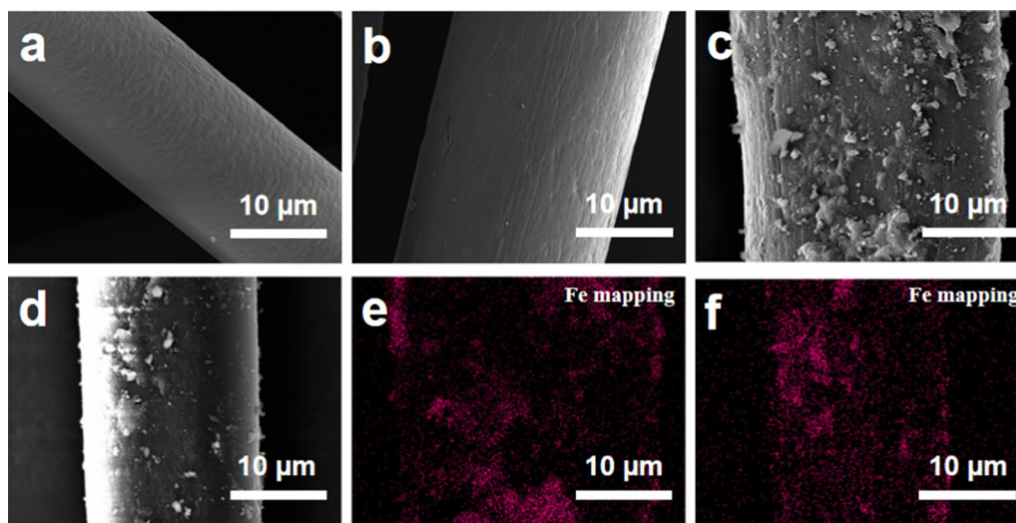


Fig. 1 SEM images of CM (a), CMBT (b), CMBT-Fe⁰ (c), CMBT-Fe⁰ after the degradation of TC (d) and the SEM-EDS Fe mapping images of CMBT-Fe⁰ before (e) and after (f) the degradation of TC

then filtered using filterable membrane (0.22 μm). The concentration of TC in the collected filtrate was measured by a UV-Vis spectrophotometer.

2.4 Characterization

The materials morphologies were observed by scanning electron microscope (SEM, Hitachi 4700, Japan). X-ray diffraction (XRD) patterns of CMBT-Fe⁰ before and after the utilization for degradation of TC were recorded on a Philips-X' Pert Pro MPD (Netherlands). The X-ray photoelectron spectrum (XPS, Shimadzu ESCA-850, Japan) of samples was recorded by using Mg-K α X-rays. XPS data were fitted by mixed Gaussian-Lorentzian functions (XPS PEAK 4.1 software). Transmission electron microscopy (TEM) images of samples were characterized using a JEOL 1200 EX-II microscope. The surface functional groups in CM, CMBT, CMBT-Fe³⁺ and CMBT-Fe⁰ before and after the utilization for degradation of TC were investigated by the Fourier transform infrared spectrometer (FTIR 920, Tianjin). The concentration of Fe³⁺ in solutions was detected by an inductively coupled plasma atomic emission spectrometer (ICP-AES, PerkinElmer Optima 2100 DV, USA).

3 Results and discussion

SEM observations shown in Fig. 1a, b confirm that the fibrous morphology of CM was well retained in the CMBT. As shown in Fig. 1c, the Fe⁰ particles in the CMBT-Fe⁰ were well-dispersed on the surface of CMBT without significant aggregation, maintaining the fibrous morphology. The successful stabilization and dispersion of Fe⁰ onto the CMBT are also confirmed by SEM-EDS

data (Fig. 1e). The fibrous morphology of CMBT-Fe⁰ after degradation of TC was well preserved (Fig. 1d). Most importantly, SEM-EDS image of CMBT-Fe⁰ after degradation of TC (Fig. 1f) indicates that the presence of CMBT effectively prevents the agglomeration of Fe⁰ particles by the rigid benzene ring skeleton and the phenolic hydroxyl groups of BT. To verify the stability of CMBT under acidic conditions, CM and CMBT were immersed in 0.2 mol/L HCl solutions for 24 h (Additional file 1: Fig. S1). CM was found to dissolve in the HCl solution. In contrast, the fibrous morphology of CMBT was maintained due to the modification of BT. These results manifest that the modification of BT to CM not only effectively suppresses the aggregation and detachment of Fe⁰ particles but also improves the stability of CM under acidic conditions.

The TEM images of CMBT-Fe⁰ before and after degradation of TC are shown in Fig. 2. The Fe⁰ nanoparticles are highly dispersed in the CMBT-Fe⁰ before and after the degradation of TC, which confirmed the critical role of BT for the stabilization of Fe⁰ nanoparticles. These results are consistent with the SEM analyses discussed above. As shown in Fig. 2c, the Fe⁰ nanoparticles exhibit well-defined lattices, with a lattice spacing of 0.2307 nm. Typical lattice spacing of Fe⁰ nanoparticles was still observed in the CMBT-Fe⁰ after the degradation of TC [30].

FT-IR spectra of CM, CMBT, CMBT-Fe³⁺, CMBT-Fe⁰ and CMBT-Fe^{0*} (the used CMBT-Fe⁰ after the degradation of TC) are shown in Fig. 3a. In the spectrum of CM, the strong broad peak at 3438.84 cm^{-1} corresponds to the stretching of O-H and N-H. The peaks observed

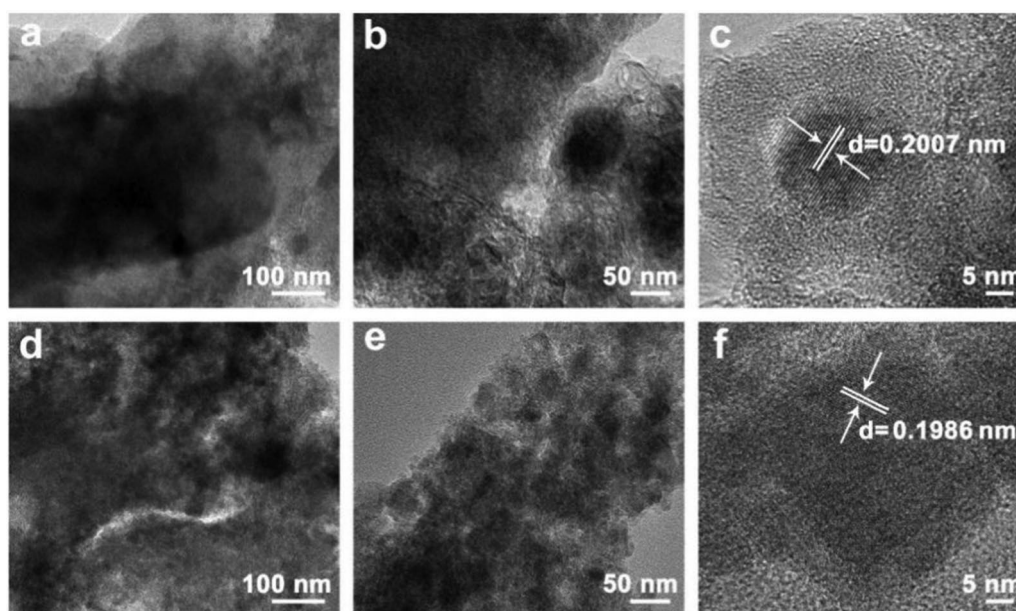


Fig. 2 TEM images of CMBT-Fe⁰ before (a–c) and after (d–f) the degradation of TC

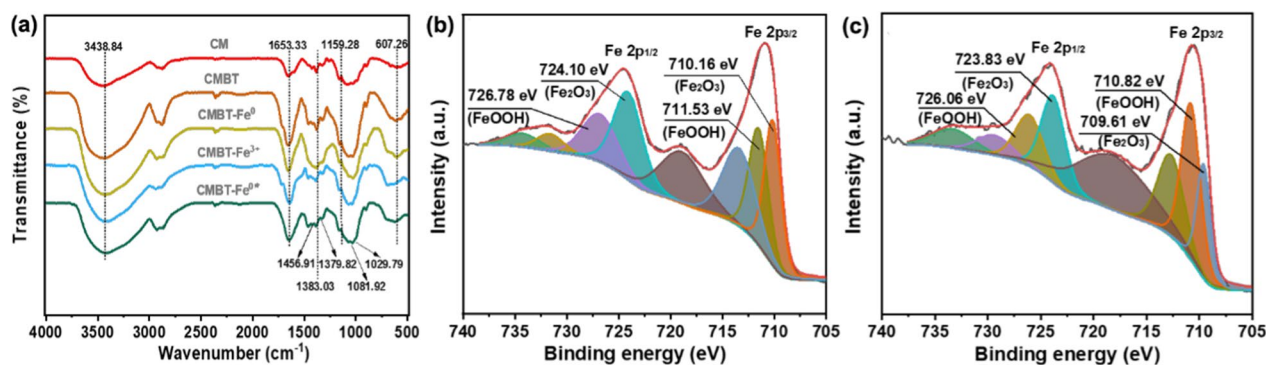


Fig. 3 FT-IR (a) and Fe 2p XPS spectra of CMBT-Fe⁰ before (b) and after (c) degradation of TC. (CMBT-Fe^{0*} in a means the obtained CMBT-Fe⁰ after the degradation of TC)

at 2921.49 cm^{-1} and 2876.49 cm^{-1} refer to the bending vibration of C–H. Amide I and II peaks are observed at 1653.33 cm^{-1} and 1383.03 cm^{-1} , respectively. The peak at 1159.28 cm^{-1} represents C–O–C stretching, while the peaks at 1081.92 cm^{-1} and 1029.79 cm^{-1} are attributed to C–O stretching and skeletal vibration of C–O stretching, respectively. In the spectrum of CMBT, the strong peak intensity at 3438.91 cm^{-1} is due to the presence of phenolic hydroxyls of BT covalently bound onto CM. The peak at 1456.91 cm^{-1} refers to the skeleton vibration of benzene ring of BT molecule. The peak at 1379.82 cm^{-1} belongs to the in-plane bending vibration absorption peak of the phenolic hydroxyls in BT molecule. These results indicate the successful

modification of CM with BT [31, 32]. In fact, the colour of CM is changed from white to brown after the modification with BT by utilizing the glutaraldehyde as the bridging agent.

Compared with the FT-IR spectrum of CMBT, only a new peak located at 607.26 cm^{-1} corresponding to the stretching vibration of Fe–O was observed in that of CMBT-Fe⁰ spectrum. The FT-IR spectra of CMBT-Fe³⁺ and CMBT-Fe⁰ showed no obvious change, indicating that the majority of functional groups containing in the CMBT are preserved after the reduction of Fe³⁺ to Fe⁰ [33].

The elemental valence state of CMBT-Fe⁰ before and after the degradation of TC were analyzed by XPS

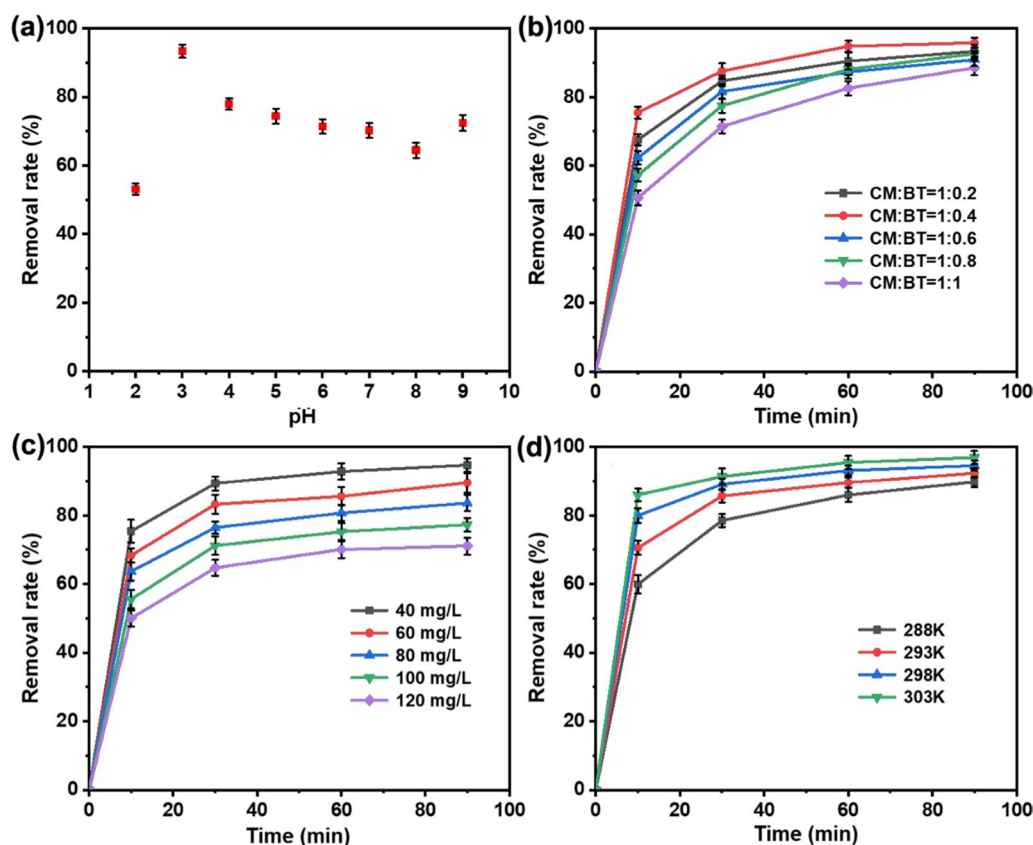


Fig. 4 Effect of pH (a), CM/BT mass ratio (b), initial concentration of TC (c) and temperature (d) on the removal performances of TC

(Fig. 3b, c and Additional file 1: Fig. S2). The XPS survey scan spectrum reveals that the CMBT-Fe⁰ is mainly composed of Fe, C, N and O. In Fig. 3b, the peaks at 710.16 and 711.53 eV are attributed to Fe₂O₃ and FeOOH, respectively, which suggests that the surface of Fe⁰ nanoparticles was oxidated during the drying process [34, 35]. The iron in the hydrolyzed state gradually increased in the CMBT-Fe⁰ after degradation of TC (Fig. 3c), which could be explained by Eq. (1).

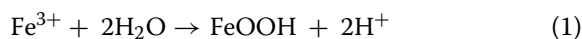


Figure 4a illustrates the influences of initial pH on the catalytic removal performances of TC. It was found that the removal rate of TC is gradually decreased with the increased pH value. 95.03% of TC was successfully removed from the solution after 90.0 min at pH 3.0, whereas only 72.35% of TC was eliminated at pH 9.0. It could be attributed to the accelerated oxidation of iron in acidic conditions, resulting in the formation of abundant activated hydrogen atoms that facilitates the reduction of TC. When the pH value is higher than 7.0, an iron hydroxide passivation layer tends to form on the surfaces of Fe⁰ nanoparticles and CMBT, which inhibits

the transport of TC and thus leads to a decrease in the removal rate of TC by the catalytic degradation.

The effect of CM/BT mass ratio to the removal performances of TC was investigated. As shown in Fig. 4b, the removal rate of TC within 90.0 min is increased from 92.93% to 95.03% as the CM/BT mass ratio is changed from 1:0.2 to 1:0.4. However, the removal rate of TC is decreased to 90.33% when the BT mass ratio is further changed from 1:0.4 to 1:1. These results suggest that the transport of TC from the solution to the Fe⁰ nanoparticles is partially hindered by the formed dense layer of BT.

The influences of reaction temperature (288–303 K) on the removal performances of TC are shown in Fig. 4c. The removal rate of TC is enhanced with the increasing temperature. The removal rate of TC shows an increase from 93.68% to 97.28% when the temperature is increased from 288 to 303 K. As shown in Fig. 4d, the removal rate of TC is declined with the increase of initial concentration from 40.0 to 120.0 mg/L. The highest removal rate of TC was achieved at the initial concentration of 40.0 mg/L, which reached 95.03% within 90 min. However, only 75.86% of TC was degraded when the initial concentration of TC was 120.0 mg/L.

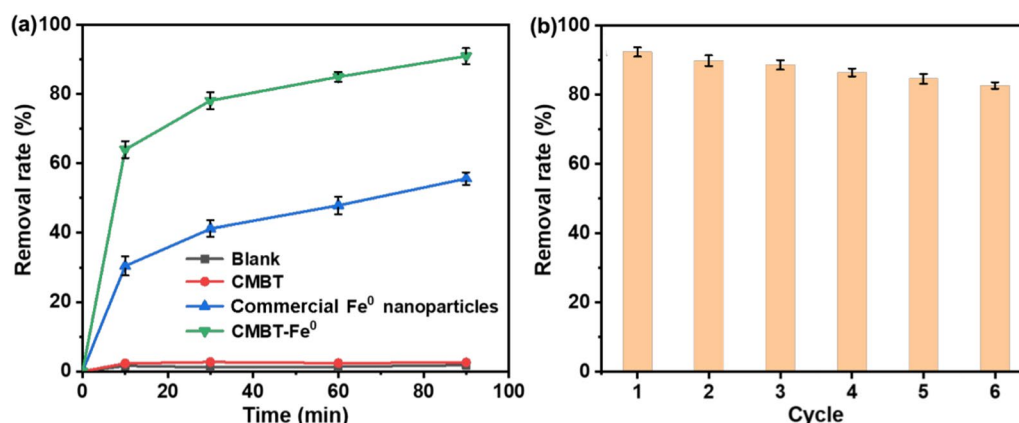


Fig. 5 Removal performances of TC by using CMBT, commercial Fe⁰ nanoparticles and CMBT-Fe⁰, respectively (a), cycling stability of CMBT-Fe⁰ for the catalytic removal of TC (b)

Figure 5a shows the removal performances of TC by using CMBT, commercial Fe⁰ nanoparticles and CMBT-Fe⁰, respectively, which obey the following order: CMBT-Fe⁰ > commercial Fe⁰ nanoparticles > CMBT. The CMBT shows quite limited removal performances to TC with ~2% of removal rate within 90 min, which manifests that Fe⁰ nanoparticles are indeed the active sites responsible for the degradation removal of TC. As for the commercial Fe⁰ nanoparticles (without the immobilization onto the CMBT), the corresponding removal rate of TC reaches 55.28% within 90 min. Compared with the commercial Fe⁰ nanoparticles, the CMBT-Fe⁰ provides considerably higher removal rate of TC, which is as high as 95.03% within 90 min, 1.72 times higher than that of the commercial Fe⁰ nanoparticles. Evidently, without the presence of CMBT, the Fe⁰ nanoparticles suffer from aggregation and/or oxidation, thus showing declined catalytic degradation removal of TC. Notably, compared with the previously reported Fe⁰ nanoparticle catalysts, the CMBT-Fe⁰ provides satisfied catalytic removal performances for the degradation of TC, as shown in Table 1.

The reusability of CMBT-Fe⁰ for the degradation removal of TC was further investigated (Fig. 5b). During the recycles, the removal rate of TC was found to

decrease gradually, while still maintaining at appreciable level. In the 6th cycle, the removal rate of TC still reaches 82.56%. These results manifest that the CMBT-Fe⁰ exhibited good cycling stability.

The intermediate products generated during the catalytic degradation removal of TC were analyzed by LC-MS (Additional file 1: Fig. S3). The degradation products were identified qualitatively, and the possible degradation route is shown in Fig. 6. The mass-to-charge ratio (*m/z*) of TC in the original solution is 444. As the degradation reaction progresses, the TC molecules are easily broken at the positions of C4 and C3 because of the low energy of the C-N bond, leading to the formation of the intermediate with the mass-to-charge ratio (*m/z*) of 381. After that, the cleavage of carboatomic ring A leads to the generation of the intermediate with the *m/z* of 305. The intermediate with the *m/z* of 275 is originated from the further decarboxylation reaction. The intermediate with the *m/z* of 245 is generated due to the subsequent dehydroxylation of the intermediate with an *m/z* of 275. Then, the cleavage of the hydroxyl in carboatomic ring B results in the formation of the intermediate with the *m/z* of 224. The intermediate with the *m/z* of 214 generates via the ring-opening reaction of carboatomic ring B. The

Table 1 Comparisons of TC degradation performances between CMBT-Fe⁰ and other catalysts

Catalyst	Dosage (g L ⁻¹)	Removal efficiency (%)	Time (h)	Concentration of TC (mg L ⁻¹)	References
CMBT-Fe ⁰	1	89	0.5	40	This work
RCL-nZVI	3	91	1	50	[36]
PDA/NZVI@BC	1	67	1.5	50	[17]
E-NZVI	0.05	91	3	50	[37]
PVP-NZVI	0.1	87	0.5	50	[16]
nZVI-Cu	0.75	72	1.5	10	[38]

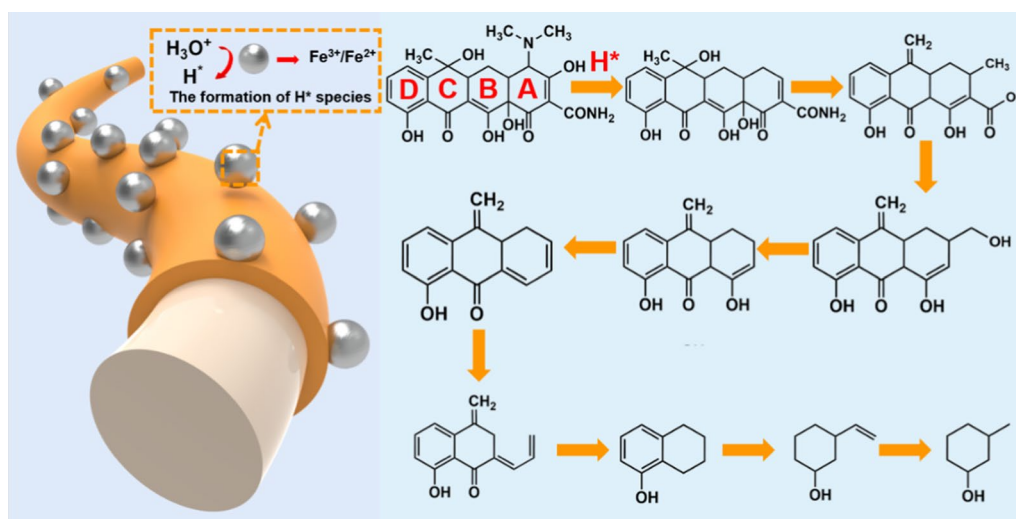


Fig. 6 Schematic illustration showing the possible degradation pathway of TC

intermediate products (with the m/z of 129 and 118) are observed as a result of losing some groups and benzene ring hydrogenation. As a consequence, the analyses to the intermediates suggest that the following reactions are involved during the catalytic degradation of tetracycline, including cleavage of carboatomic ring A, decarboxylation, dehydroxymethylation and hydrogenation of benzene ring [39, 40].

4 Conclusions

In summary, the CMBT-Fe⁰ catalyst successfully developed by the inspiration of combination tanning mechanism displayed high activity and cycling stability for the catalytic removal of tetracycline. The CMBT-Fe⁰ was capable of providing the removal rate of TC as high as 95.03%, which was 1.72 times higher than that of commercial Fe⁰ nanoparticles without immobilization. The CMBT-Fe⁰ catalyst also showed satisfactory recycling performances, with 82.56% of removal rate to TC in the 6th cycle. Furthermore, a possible catalytic degradation removal mechanism was also proposed.

Supplementary Information

The online version contains supplementary material available at <https://doi.org/10.1186/s42825-023-00130-w>.

Additional file 1: Fig. S1. Photographs of CM and CMBT after immersion in 0.2 mol/L HCl for 24 h. **Fig. S2.** XPS survey scan spectra of CMBT-Fe⁰ before (a) and after (b) the degradation of TC. **Fig. S3.** Mass spectrum of TC (a), mass spectra of TC degraded by CMBT-Fe⁰ for 30 min (b) and 90 min (c), respectively.

Author contributions

MX: Investigation, Methodology, Writing-original draft. SL: Investigation. WQ: Investigation. YP: Investigation, Methodology. QY: Writing-review,

Methodology. HM: Conceptualization, Writing-review & editing, Supervision, Funding acquisition.

Funding

This work was financially supported by National Key R&D Program of China (2021YFC2103800), the Technical Development Project of Sichuan University (No.22H0798) and Fundamental Research Funds for the Central Universities.

Availability of data and materials

All data from this study are presented in the paper and the supplementary material.

Declarations

Competing interests

The authors declare that they have no known competing financial interests or personal relationships that could have appeared to influence the work reported in this paper. Qingyu Yan is a member of the editorial board of *Collagen and Leather*, and was not involved in the editorial review, or the decision to publish this article. All authors declare that there are no competing interests.

Author details

¹College of Chemical Engineering, Sichuan University, Chengdu 610065, People's Republic of China. ²College of Chemistry and Materials Science, Sichuan Normal University, Chengdu 610066, People's Republic of China. ³School of Materials Science and Engineering, Nanyang Technological University, Singapore 639798, Singapore.

Received: 14 July 2023 Revised: 14 August 2023 Accepted: 17 August 2023

Published online: 23 August 2023

References

- Selmi T, Sanchez-Sanchez A, Gadonneix P, Jagiello J, Seffen M, Sammouda H, Celzard A, Fierro V. Tetracycline removal with activated carbons produced by hydrothermal carbonisation of *Agave americana* fibres and mimosa tannin. *Ind Crop Prod*. 2018;115:146–57. <https://doi.org/10.1016/j.indcrop.2018.02.005>.
- Liao Q, Rong H, Zhao M, Luo H, Chu Z, Wang R. Interaction between tetracycline and microorganisms during wastewater treatment: a review.

- Sci Total Environ. 2021;757:143981. <https://doi.org/10.1016/j.scitotenv.2020.143981>.
- Auerbach EA, Seyfried EE, McMahon KD. Tetracycline resistance genes in activated sludge wastewater treatment plants. *Water Res.* 2007;41:1143–51. <https://doi.org/10.1016/j.watres.2006.11.045>.
 - Zhang P, Li Y, Cao Y, Han L. Characteristics of tetracycline adsorption by cow manure biochar prepared at different pyrolysis temperatures. *Bioresour Technol.* 2019;285:121348. <https://doi.org/10.1016/j.scitotenv.2020.143981>.
 - Rigueto CVT, Rosseto M, Krein DDC. Alternative uses for tannery wastes: a review of environmental, sustainability, and science. *Collagen Leather.* 2020;2:21. <https://doi.org/10.1186/s42825-020-00034-z>.
 - Wu S, Hu H, Lin Y, Zhang J, Hu Y. Visible light photocatalytic degradation of tetracycline over TiO₂. *Chem Eng J.* 2020;382:122842. <https://doi.org/10.1016/j.cej.2019.122842>.
 - Chang Q, Ali A, Su J, Wen Q, Bai Y, Gao Z. Simultaneous removal of nitrate, manganese, and tetracycline by *Zoogloea* sp. MFQ7: adsorption mechanism of tetracycline by biological precipitation. *Bioresour Technol.* 2021;340:125690. <https://doi.org/10.1016/j.biortech.2021.125690>.
 - Fu Y, Peng L, Zeng Q, Yang Y, Song H, Shao J, Liu S, Gu J. High efficient removal of tetracycline from solution by degradation and flocculation with nanoscale zerovalent iron. *Chem Eng J.* 2015;270:631–40. <https://doi.org/10.1016/j.cej.2015.02.070>.
 - Wang X, Zhang B, Ma J, Ning P. Novel synthesis of aluminum hydroxide gel-coated nano zero-valent iron and studies of its activity in flocculation-enhanced removal of tetracycline. *J Environ Sci.* 2020;89:194–205. <https://doi.org/10.1016/j.jes.2019.09.017>.
 - Zha S, Cheng Y, Gao Y, Chen Z, Megharaj M, Naidu R. Nanoscale zero-valent iron as a catalyst for heterogeneous Fenton oxidation of amoxicillin. *Chem Eng J.* 2014;255:141–8. <https://doi.org/10.1016/j.cej.2014.06.057>.
 - Xiao M, Qi W, Jia S, Pang M, Shi F, Mao H. High-performance removal of tetracycline enabled by Fe⁰ nanoparticles supported on carbon@ZIF-8. *Chem Res Chin U.* 2022;38(6):1349–55. <https://doi.org/10.1007/s40242-022-2255-y>.
 - Nadagouda MN, Castle AB, Murdock RC, Hussain SM, Varm RS. In vitro biocompatibility of nanoscale zerovalent iron particles (NZVI) synthesized using tea polyphenols. *Green Chem.* 2010;12:114–22. <https://doi.org/10.1039/B921203P>.
 - Astruc D. The supramolecular redox functions of metallomacromolecules. *Collagen Leather.* 2020;2:13. <https://doi.org/10.1186/s42825-020-00026-z>.
 - Sun Z, Zheng S, Ayoko GA, Frostb RL, Xi Y. Degradation of simazine from aqueous solutions by diatomite-supported nanosized zero-valent iron composite materials. *J Hazard Mater.* 2013;263:768–77. <https://doi.org/10.1016/j.jhazmat.2013.10.045>.
 - Baldermann A, Kaufhold S, Dohrmann R, Baldermann C, Letofsky-Papst I, Dietzel M. A novel nZVI–bentonite nanocomposite to remove trichloroethene (TCE) from solution. *Chemosphere.* 2021;282:131018. <https://doi.org/10.1016/j.chemosphere.2021.131018>.
 - Chen H, Luo H, Lan Y, Dong T, Hu B, Wang Y. Removal of tetracycline from aqueous solutions using polyvinylpyrrolidone (PVP-K30) modified nanoscale zero valent iron. *J Hazard Mater.* 2011;192:44–53. <https://doi.org/10.1016/j.jhazmat.2011.04.089>.
 - Wang X, Lian W, Sun X, Ma J, Ning P. Immobilization of NZVI in polydopamine surface-modified biochar for adsorption and degradation of tetracycline in aqueous solution. *Front Env Sci Eng.* 2018;12:1–11. <https://doi.org/10.1007/s11783-018-1066-3>.
 - Dong H, Zhao F, He Q, Xie Y, Zeng Y, Zhang L, Tang L, Zeng G. Physico-chemical transformation of carboxymethyl cellulose-coated zero-valent iron nanoparticles (nZVI) in simulated groundwater under anaerobic conditions. *Sep Purif Technol.* 2017;175:376–83. <https://doi.org/10.1016/j.seppur.2016.11.053>.
 - Sun Y, Jing R, Zheng F, Zhang S, Jiao W, Wang F. Evaluating phytotoxicity of bare and starch-stabilized zero-valent iron nanoparticles in mung bean. *Chemosphere.* 2019;236:124336. <https://doi.org/10.1016/j.chemosphere.2019.07.067>.
 - Sun M, Zhang Z, Liu G, Lv M, Feng Y. Enhancing methane production of synthetic brewery water with granular activated carbon modified with nanoscale zero-valent iron (NZVI) in anaerobic system. *Sci Total Environ.* 2021;760:143933. <https://doi.org/10.1016/j.scitotenv.2020.143933>.
 - Yang Y, Xu L, Shen H, Wang J. Construction of three-dimensional reduced graphene oxide wrapped nZVI doped with Al₂O₃ as the ternary Fenton-like catalyst: Optimization, characterization and catalytic mechanism. *Sci Total Environ.* 2021;780:146576. <https://doi.org/10.1016/j.scitotenv.2021.146576>.
 - Cirtiu CM, Raychoudhury T, Ghoshal S, Moores A. Systematic comparison of the size, surface characteristics and colloidal stability of zero valent iron nanoparticles pre- and post-grafted with common polymers. *Colloid Surf A.* 2011;390:95–104. <https://doi.org/10.1016/j.colsurfa.2011.09.011>.
 - Nieto-Zambrano S, Ramos-Ramírez E, Morales FT, Boffito DC, Naccache R, Ortega NLG, Litter MI, Cipagauta-Díaz S, Barbosa-Lopez AL. ZnAl hydroxaltes modified with nanocomposites nZVI–PAA for environmental remediation. *J Mater Res Technol.* 2021;14:2243–56. <https://doi.org/10.1016/j.jmrt.2021.06.055>.
 - Kou SG, Peters LM, Mucalo MR. Chitosan: A review of sources and preparation methods. *Int J Bio Macromol.* 2021;169:85–94. <https://doi.org/10.1016/j.ijbiomac.2020.12.005>.
 - Ahmed S, Ikram S. Chitosan based scaffolds and their applications in wound healing. *Achiev Life Sci.* 2016;10:27–37. <https://doi.org/10.1016/j.als.2016.04.001>.
 - Ragety GR, Griffon DJ, Lee HB, Chung YS. Effect of collagen II coating on mesenchymal stem cell adhesion on chitosan and on reacylated chitosan fibrous scaffolds. *J Mater Sci-Mater Med.* 2010;21:2479–90. <https://doi.org/10.1007/s10856-010-4096-3>.
 - Yeul VS, Rayalu SS. Unprecedented chitin and chitosan: a chemical overview. *J Polym Environ.* 2013;21:606–14. <https://doi.org/10.1007/s10924-012-0458-x>.
 - Zhang Z, Liu Y, Wang J, Xie T, Sun L, Li Z. A chrome-free combination tanning strategy: based on silicic acid and plant tannin. *Collagen Leather.* 2021;3:1–13. <https://doi.org/10.1186/s42825-021-00058-z>.
 - Huang X, Wu H, Pu S, Liao X, Shi B. One-step room-temperature synthesis of Au@Pd core–shell nanoparticles with tunable structure using plant tannin as reductant and stabilizer. *Green Chem.* 2011;13:950–7. <https://doi.org/10.1039/C0GC00724B>.
 - Wang B, Sun J, Abbas M, Liu Y, Kong F, Xiao H, Chen J. A novel hydrothermal approach for the synthesis of flower-like Fe₂O₃/Fe foam nanocrystals and their superior performance in fisher–tropsch synthesis. *Catal Lett.* 2017;147:1153–61. <https://doi.org/10.1016/j.carbon.2016.09.026>.
 - Pawlak A, Mucha M. Thermogravimetric and FTIR studies of chitosan blends. *Thermochim Acta.* 2003;396:153–66. [https://doi.org/10.1016/S0040-6031\(02\)00523-3](https://doi.org/10.1016/S0040-6031(02)00523-3).
 - Chupin L, Motillon C, Charrier-El Bouhtoury F, Pizzi A, Charrier B. Characterisation of maritime pine (*Pinus pinaster*) bark tannins extracted under different conditions by spectroscopic methods, FTIR and HPLC. *Ind Crop Prod.* 2013;49:897–903. <https://doi.org/10.1016/j.indcrop.2013.06.045>.
 - Das PK, Mitra K, Dey A. Spectroscopic characterization of a phenolate bound Fe II–O₂ adduct: gauging the relative “push” effect of a phenolate axial ligand. *Chem Commun.* 2014;50:5218–20. <https://doi.org/10.1039/C3CC47528J>.
 - Ma Y, Wang B, Wang Q, Xing S. Facile synthesis of α -FeOOH/ γ -Fe₂O₃ by a pH gradient method and the role of γ -Fe₂O₃ in H₂O₂ activation under visible light irradiation. *Chem Eng J.* 2018;354:75–84. <https://doi.org/10.1016/j.cej.2018.08.011>.
 - Qin Q, Liu T, Zhang J, Wei R, You S, Xu Y. Facile synthesis of oxygen vacancies enriched α -Fe₂O₃ for peroxymonosulfate activation: a non-radical process for sulfamethoxazole degradation. *J Hazard Mater.* 2021;419:126447. <https://doi.org/10.1016/j.jhazmat.2021.126447>.
 - Abdelfatah AM, Fawzy M, El-Khouly ME, Abdelazeem SE. Efficient adsorptive removal of tetracycline from aqueous solution using phytosynthesized nano-zero valent iron. *J Saudi Chem Soc.* 2021;12:101365. <https://doi.org/10.1016/j.jscs.2021.101365>.
 - Wang X, Wang X, Lynch I, Ma J. High-efficiency removal of tetracycline from water by electrolysis-assisted NZVI: mechanism of electron transfer and redox of iron. *RSC Adv.* 2023;23:15881–91. <https://doi.org/10.1039/D3RA00954H>.
 - Gopal G, Sankar H, Natarajan C, Mukherjee A. Tetracycline removal using green synthesized bimetallic nZVI–Cu and bentonite supported green nZVI–Cu nanocomposite: a comparative study. *J Environ Manag.* 2020;254:109812. <https://doi.org/10.1016/j.jenvman.2019.109812>.

39. Cao J, Xiong Z, Lai B. Effect of initial pH on the tetracycline (TC) removal by zero-valent iron: adsorption, oxidation and reduction. *Chem Eng J.* 2018;343:492–9. <https://doi.org/10.1016/j.cej.2018.03.036>.
40. Li Y, Sun X, Tang Y, Ng YH, Li L, Jiang F, Wang J, Chen W, Li L. Understanding photoelectrocatalytic degradation of tetracycline over three-dimensional coral-like ZnO/BiVO₄ nanocomposite. *Mater Chem Phys.* 2021;271:124871. <https://doi.org/10.1016/j.matchemphys.2021.124871>.

Publisher's Note

Springer Nature remains neutral with regard to jurisdictional claims in published maps and institutional affiliations.

Submit your manuscript to a SpringerOpen[®] journal and benefit from:

- ▶ Convenient online submission
- ▶ Rigorous peer review
- ▶ Open access: articles freely available online
- ▶ High visibility within the field
- ▶ Retaining the copyright to your article

Submit your next manuscript at ▶ [springeropen.com](https://www.springeropen.com)
